Performance Evaluation of Hybrid Power System Incorporating Electric-Vehicles

Sheikh Safiullah and Asadur Rahman*

Electrical Engineering Department, National Institute of Technology Srinagar, J&K, India
E-mail: asadur2003@yahoo.co.in
**Corresponding Author*

Received 07 November 2021; Accepted 06 February 2022;
Publication 22 April 2022

Abstract

State-of-the-art: The present study broadly addresses the performance analysis of a hybrid power system with the inclusion of modern day electric vehicles (EV) and renewable energy sources. Generations in the form of conventional-thermal, diesel-plant, solar-thermal for the hybrid power system as well as EVs establish a concurrent regulation of system frequency, voltage and corresponding tie-lie power. The effective power management for the power system is established in such a way that EV realizes the battery management system integrated with the utility grid. The instantaneous control and management capability of a grid-connected EV are the main attractive features that are highlighted in this work. Small signal stability study of the developed hybrid power system is investigated through Eigen-value analysis.

Methods & Outcomes: For anticipated performance enhancement for the developed hybrid power system, the parameters are adjusted using a dominant magnetotactic-bacteria optimization (MBO) technique. The performance of MBO optimized controller for effective control of system dynamic responses are validated in this study. Sensitivity tests involving large deviations beyond nominal values of system components validate the reliability of the hybrid power system. The role of EV in terms of power control and management has

Distributed Generation & Alternative Energy Journal, Vol. 37_4, 1055–1082.
doi: 10.13052/dgaej2156-3306.3748

been successfully demonstrated. The stability of the controlled power system is verified using Eigen-value analysis. The role of EVs help to improve system stability is also proved.

Keywords: Hybrid power system, load frequency control (LFC), integral double derivative (IDD) controller, electric vehicle (EV), magnetotactic bacteria optimization (MBO), automatic voltage regulator (AVR).

1 Introduction

Due to environmental issues and threats to energy security, renewable energy schemes have since long been extensively established in several countries during past years. Pertaining to this challenge, enormous quantities of renewable energy sources are incorporated in power systems which deliver innovative challenges and prospects for the process and planning of networks. Presently, renewable energy resources combined with conventional generators deliver different natures of power system supplementary tasks like load frequency control (LFC), automatic voltage regulator (AVR) etc. The system frequency strength of a network has a direct relationship with the active and reactive power of the network respectively. Any change in frequency or voltage from the scheduled values might cause the equipment in power system to behave abnormally. Pertaining to this area, extensive works have been done on LFC and AVR systems.

1.1 Related Literature and Key Gaps

Diverse control technologies have been projected in literature pertaining to a multi-area power system using renewable sources. The integration of renewable energy sources with the utility grid received huge attention like Ting Wu et al. in [1] have proposed a grid-connected integrated energy system considering biogas-solar-wind renewables. Fukang Ren et al. studied a hybrid combined cooling-heating power system renewable energy resources [2]. Notably, various works have been reported in literature for system frequency regulation using renewable resources as well. The initial study on multi-area system is described by Elgerd et al. [3]. Farooq Z in [4] have performed the load frequency control of hybrid power system using various renewable sources incorporated in the system. Authors in [5–7] have analyzed the impact of renewable energy sources for a multi-area power system. Rahman et al. [8] presented the dynamic control of a hybrid two area power system.

Similarly, Rahman et al. [9] reported the LFC of a multi-area system using cuckoo search optimization technique. Wei et al. [10] proposed the optimal LFC approach of an interconnected power system using photo-voltaic plants. Rahman et al. [11] have presented the LFC of hydro-thermal system under deregulated conditions. Swati Sondhi et al. have LFC of an interconnected power system [12]. We Tan [13] has also studied the LFC of a multi-area power system. The literature reported in [1–13] are mainly focused on frequency control and voltage control studies of multi-area power system separately. Very few literatures are present based on the collective operation of effective frequency and voltage control. Rumi et al. [14] presented the combined frequency and tie-line power control in addition to the voltage control in a hybrid power system. Similarly, authors in [15, 16] have studied the combined frequency-voltage operation of hybrid system using various renewable energy sources. Hence, more work is to be done in the present area.

Nowadays, various works are done in this field regarding integration of EVs in multi-area power system. H. Neves et al. [17] proposed a smart controllable EV battery charger with vehicle-to-grid interaction capability. Lee et al. [18] proposed a theoretical analysis for EV charging systems using renewable power generators. Similarly, Rami Abousleiman et al. [19] implemented smart charging design for interactive EV and power grid systems. Saha et al. [20] studied the integration of LFC with EV using cascaded controller. H. Liu et al. [21] described the control of EV-to-grid for frequency stabilization using high frequency signals under real-time conditions. Fabian Kennel et al. [22] presented the energy management of smart grids using EVs. Hanaan et al. [23] proposed a multi-source model for energy management for EVs. In this view, a further detailed study on incorporation of EVs in combined LFC-AVR operation (as reported in previous paragraph) for better system performance needs to be done.

Frequency and voltage investigations with classical controllers have received a lot of attention. The authors in [4, 22] compared the dynamic response corresponding to classical controllers Integral (I), Proportional-Integral (PI), Proportional-Integral-derivative (PID). Rumi et al. [14] compared performance of classical controllers with respect to Integral-double Derivative-Frational (IDDF) controller. R. K. Sahu [19] et al. studied PI/PIDF controllers in their study. Morsali et al. [20] incorporated fractional order PID interconnected multi-source power system. Similarly, various studies based on the use of controllers have been published in this sector. Aside from this, multi-area power system research incorporates a variety of modified

complicated controllers. Integral minus proportional derivative controllers were presented by Kler et al. [21]. In the LFC investigation, S. Debbarma proved the usage of fractional order ID. A cascaded PID controller has been simulated in [23]. Cascaded controllers like PI-PD in load frequency control are demonstrated in [24] and PD-PID in [25]. However, simple control procedures are advised to prevent further complexity, and so integral-double-derivative (IDD) as secondary controller is utilized for the present study. The motivation for incorporation of IDD controller is discussed in Section 1.3.

The secondary controller gains and other parameters must be adjusted by an appropriate optimization algorithm for stable operation of the power system. The pace of convergence and precision of optimal values determine an algorithm's performance. The genetic algorithm (GA) is a limited optimization approach that is both efficient and effective [3]. In comparison to GA, the bacteria foraging (BF) optimization process requires more search space parameters. The particle swarm optimization (PSO) algorithm approach has a poor convergence rate [3]. Rumi et al. [10] presented an LSA-optimized approach to manage multi-area frequency and voltage control. Dash et al. [26] demonstrated bat algorithm technique for optimization of cascaded controllers. Rahman et al. [27] have successfully applied biogeography based optimization technique for ALFC of a hydro-thermal system. Nayak et al. [28] have applied hybrid salp-algorithm algorithm for the optimization of gains of all the controllers. A highly efficient and accurate magnetotactic bacteria optimization (MBO) technique is available in the literature [29]. The present work applies MBO technique for real-time optimization of gains values of controller and coupling coefficient in the combined LFC-AVR studies.

1.2 Contributions of Present Studies

Based on the above studies, the major contributions related to present work are:

1. Performance analysis of incorporation of renewable energy sources and modern day EVs for a hybrid power system based on concurrent control of system frequency, voltage and corresponding tie-line power is analyzed.
2. The role of EVs for energy control, management and system regulation for improvement of power system dynamic characteristics is studied.
3. In order to assess the stability of the developed hybrid power system, Eigen value analysis is carried.

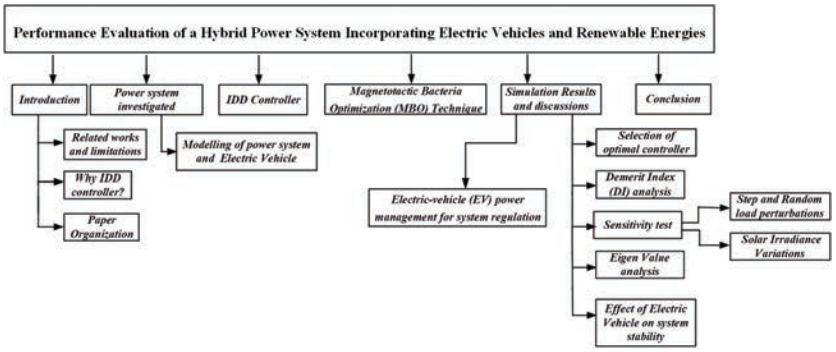

Figure 1 Overview of the paper.

1.3 Objectives Related to the Present Work

Pertaining to the studies carried above, the present work objectives are as follows:

1. To design a hybrid power system incorporating electric vehicles (EVs) and renewable energy sources for frequency and voltage regulation.
2. To choose an optimal controller available in literature as secondary controller for the developed system and verify its optimality by comparing the system dynamic characteristics.
3. To illustrate the role of EV for energy control, management and system regulation.
4. To verify the stability of optimal controlled system using Eigen value analysis.
5. To assess the system performance in presence of EVs.
6. To test the disturbance handling capability of the power system using sensitivity analysis.

1.4 Paper Organization

The manuscript content and overview of the topics which are discussed in present study is shown in Figure 1.

2 Research Method

The present work is validated by testing the performance of the developed hybrid power system, controller and optimization technique in MATLAB Simulink software which are explained as below.

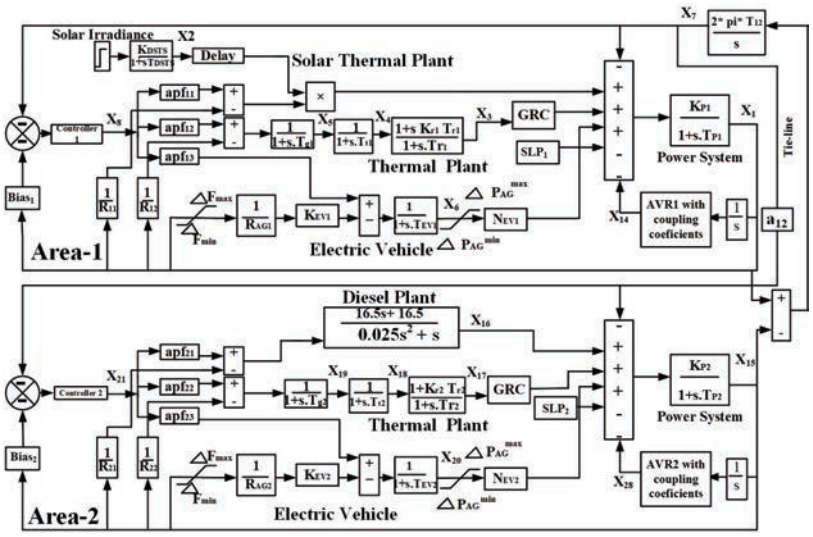

Figure 2 Transfer function (T.F) for joint LFC-AVR power system.

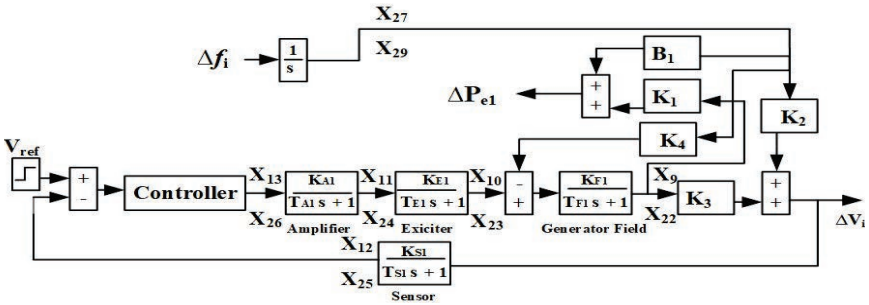

Figure 3 T.F of automatic voltage regulator.

2.1 Design and Modeling of Electrical Power System (Objective 1 of Section 1.3)

Figure 2 shows a two-area multi-source power system transfer function model for collective operation of LFC and AVR integrating EVs. The area capacity ratio is considered as 2:3. Figure 3 illustrates the AVR implementation for every given area. Area 1 consists of a thermal unit, a solar-thermal unit and EV to grid integration. Area 2 is composed of diesel plant, thermal plant and electric vehicles. Dead band and rate limits are taken into account in the thermal plants [18]. The utility grid presently trends for incorporating EV. The charging and discharging proportion and capabilities of EVs are

scheduled within industry standards to keep the grid balanced. The power system becomes realistic when all of the above factors are combined.

For dynamic analyses of the system, a 1% step load perturbation (SLP) in area-1 is supplied. The nominal values of the system are taken from [10] and [14]. The MBO approach for controller gain is used to simulate the power system in the MATLAB® Simulink environment. Several objective functions for the minimization or maximization of the processes have been presented in the literature. Various objective functions such as Integral Time Absolute Error (ITAE) analysis, Integral Absolute Error (IAE) analysis, Integral Time Square Error (ITSE) analysis and Integral Square Error (ISE) evaluation are available for the study when considering frequency deviation and deviation in tie-line power for ith-area. ISE, on the other hand, has elements of both ITSE and ITAE [23]. Hence, ISE is used as objective function in the present work.

$$ISE = \int_0^T [(\Delta f_i)^2 + (\Delta P_{tie})^2 + (\Delta V_i)^2]dt \tag{1}$$

2.2 Electric Vehicle (EV) Modelling

The collective simulation-model of EV used in the present work is displayed in Figure 4. The main purpose of battery charge management (BCM) system (Figure 4) is to sustain the grid to battery power interchange. Sometimes, due to unavoidable conditions, EVs may unpredictably get detached which will result in unsatisfactory response of the system. This condition is overcome by limiting the system frequency inside a defined band of ± 10 mHz. The charging & discharging process of EV determines its capacity, which is directly related to the amount of regulation capability task fulfilled by the EVs [15]. The capacity of power-load determines the regulatory management. Furthermore, EVs contributing to regulatory responsibilities require enough time for battery charging to the anticipated level. As a result, the charging and

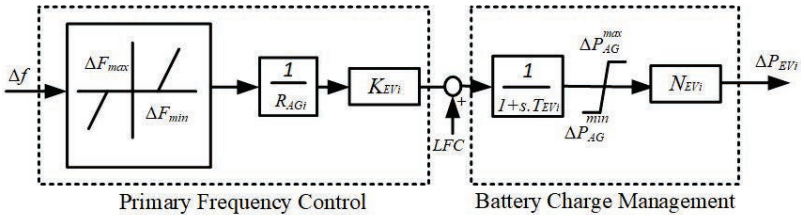

Figure 4 Simulation model of EV.

discharging management job must stay within the EV's capacity restrictions. As a result, the charging and discharging capacity of EVs is restricted to a range of -5 kW to $+5$ kW. Because all producing units, including EVs are responsible for regulation, any power discrepancy will be split into two portions. All of the producing units in a given region will do one portion of the work, while BCM will handle the rest. BCM gain is taken as $\mathrm{K_{EVi}}$ while the time constant of BCM is $\mathrm{T_{EVi}}$. The value for droop coefficient (R_{AG}) is 2.4 Hz/p.u (Figure 4). ΔP_{EVi} denotes the regulation power-change for EV. P_{AG}^{max} being maximum output power while P_{AG}^{min} represents minimum power output of EV which are calculated using Equations (2) and (3).

$$P_{AG}^{max} = + \left[\frac{1}{N_{EV}} \times (\Delta P_{EVi}) \right] \tag{2}$$

$$P_{AG}^{min} = - \left[\frac{1}{N_{EV}} \times (\Delta P_{EVi}) \right] \tag{3}$$

N_{EV} signifies number of electric vehicles connected.

2.3 Integral-Double-Derivative-(IDD)-Controller

IDD, as secondary controller, is presented by Saikia et al. [30] and have compared its effectiveness with other conventional controllers. The double-derivative component of IDD has better outcomes than single derivative by decreasing high frequency noise due to the system disturbances and fluctuations in the output. Area-control-error (ACE), which consists of a variation in tie-line power ($\Delta \mathrm{P_{tie}}$) and a variation in frequency (Δf), is given to the controller as an input in the LFC loop. While in AVR, voltage error (ΔV) is taken as input. Figure 5 gives the representation of a conventional IDD controller. The input area-control-error for LFC system for any area 'i' is denoted using Equation (4). The equation representing the transfer-function

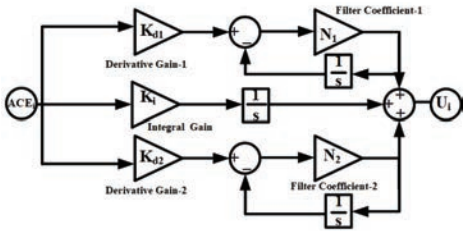

Figure 5 Block diagram of IDD controller.

for IDD-controller is given by (5).

$$ACE_i = B_i * \Delta f_i + \Delta P_{tie} \tag{4}$$

$$U_i(s) = \frac{K_i(s)}{s} + sK_{d1}(s) \Big/ \frac{1}{sN_1 + 1} + sK_{d2}(s) \Big/ \frac{1}{sN_2 + 1} \tag{5}$$

2.3.1 Why IDD controller?

The literatures in [4–7, 10, 18] mentioned above have studied classical controllers in multi-area power system studies. Similarly, [19–22] have incorporated more intricate controllers in their studies. In [23, 24], and [25], the multi-area power system is also exposed to complicated cascaded controllers. However, it is worth noting that an interconnected power network is fundamentally complex in nature and the inclusion of more intricate schemes in the form of a controller increases to its complexity, confounding system response regulating approaches. Why add to the system's complexity when there are already some easier approaches? Furthermore, traditional control techniques such as I, P, PI, PID and others are a thing of the past. As a result, a simple IDD controller is used as a secondary controller in the current analysis.

2.4 Magnetotactic Bacteria Optimization (MBO) Technique (Objective 2 of Section 1.3)

Hongwei Mo and Lifang Xu [29] introduced the MBO technique. This technique relies on the magnetotactic bacteria's (MTB) properties. MBO is a unique optimization approach inspired by MTB biological characteristics. Throughout their evolution, MTB cells have reinvented in reaction to modifications in the magnetic exposure. Such cells possessing magnetosomes can alter magnetic field forces to minimize magnetotactic energy.

MTBs have acquired a susceptibility to shift the magnetic line of axis course using assistance of magnetosomes in order to survive in nature. This is essential for MTBs to lower the magnetotactic energy, which is growing in nature. With this, by continually controlling the moments of each cell, the MBO technique produces the greatest results. Flowchart in Figure 6 depicts the gist of MBO technique.

The authors in [29] have tested MBO on multimodal functions and compared the outcome with existing techniques. Experimental results in [29] indicate that MBO is exceedingly fruitful in optimization processes and overtakes supplementary algorithms by a significant margin. MBO is compared to Genetic Algorithm (GA), Particle Swarm Algorithm (PSO),

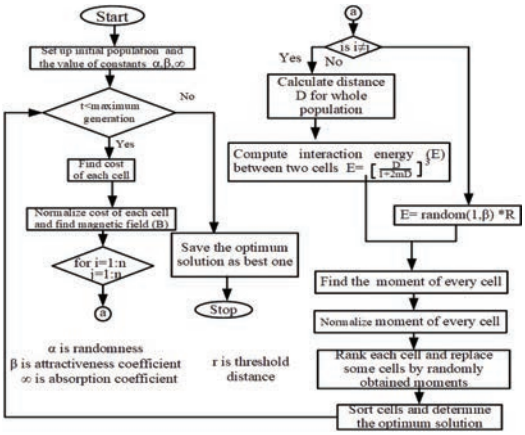

Figure 6 Flowchart of MBO technique.

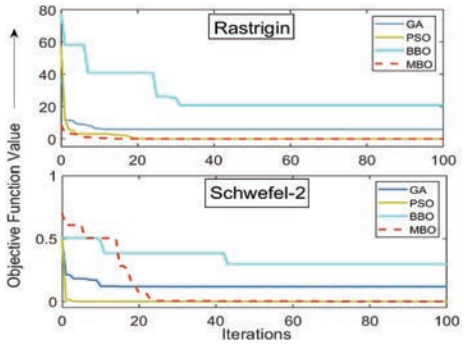

Figure 7 Convergence of Schwefel and Rastrigin-2 function.

Biogeography-based optimization (BBO) in terms of convergence for some mathematical benchmark functions (Schwefel & Rastrigin). Figure 7 shows that MBO outdoes PSO, GA & BBO in terms of minimizing test function values and challenges GA, PSO, and considerably improved than BBO.

3 Results and Discussion

The MATLAB® Simulink is used to model the developed hybrid power system. The system is provided with 1 percent SLP in area-1 and solar irradiation varying from 600 W/m^2 to 800 W/m^2 at a 50-second step time under ideal conditions. The optimization of coupling coefficients of AVR loop and the controller gains is done utilizing MBO technique.

3.1 Evaluation of Optimum Controller for Nominal Conditions: (Objective 3 of Section 1.3)

In LFC-AVR operation of power system, many standard controllers in the form of I, ID, PI, PID and Integral double derivative (IDD) are used one by one. For LFC functioning, two controllers are deployed for each control area. For each AVR, separate controller is provided. In combined LFC-AVR operation, the location of all four controllers is as depicted in Figures 2–3. Simultaneous optimization of coupling coefficients for AVR in both areas is carried out using MBO technique and reported in Table 1. Table 2 shows the MBO optimized gain settings for several controllers, considered one at a time. Responses for frequency variations, voltage deviations, and tie-line power deviations are accomplished in both areas. Figure 8 shows the dynamic responses that are obtained following simulation and are analyzed for comparison. The dynamic response analysis for comparison discloses that IDD is acting as the optimal controller. This partially attains objective 3 of the Section 1.3.

To authenticate the execution of MBO technique for the present work, the controller in the present hybrid energy system is optimized and compared for different optimization techniques available in literature. The IDD controller is used as the reference controller and ISE as the objective function for all the techniques. The performance of MBO is compared with several optimization techniques viz. GA, PSO, BBO and Firefly Algorithm (FA). Figure 9 shows

Table 1 Optimized values of coupling coefficient for AVR in area-1 and area-2

Parameter	AVR in Area-1	AVR in Area-2
B_1	0.3592	0.3549
K_1	0.1836	0.1749
K_2	−0.1930	−0.1966
K_3	0.1258	0.1165
K_4	0.0098	0.0012

Table 2 Optimized gains for different controllers

	K_i				K_d				N				K_p			
Controller	K_{i1}	K_{i2}	K_{i3}	K_{i4}	K_{d1}	K_{d2}	K_{d3}	K_{d4}	N_1	N_2	N_3	N_4	K_{p1}	K_{p2}	K_{p3}	K_{p4}
I	0.19	0.47	0.49	0.02	–	–	–	–	–	–	–	–	–	–	–	–
ID	0.35	0.66	0.42	0.84	1.67	0.51	1.23	1.16	54.1	86.9	26.5	31.8	–	–	–	–
PI	0.43	0.65	0.10	0.93	–	–	–	–	–	–	–	–	0.19	0.23	0.79	0.49
PID	0.11	1.76	1.69	1.14	1.04	0.99	1.66	0.03	41.1	31.3	22.6	43.1	0.92	0.13	0.77	1.48
IDD	0.19	0.49	0.16	0.39	0.98	0.32	0.28	0.45	89.8	88.6	54.9	68.4	–	–	–	–
					0.32	0.18	0.50	0.66	52.5	57.8	59.6	39.7				

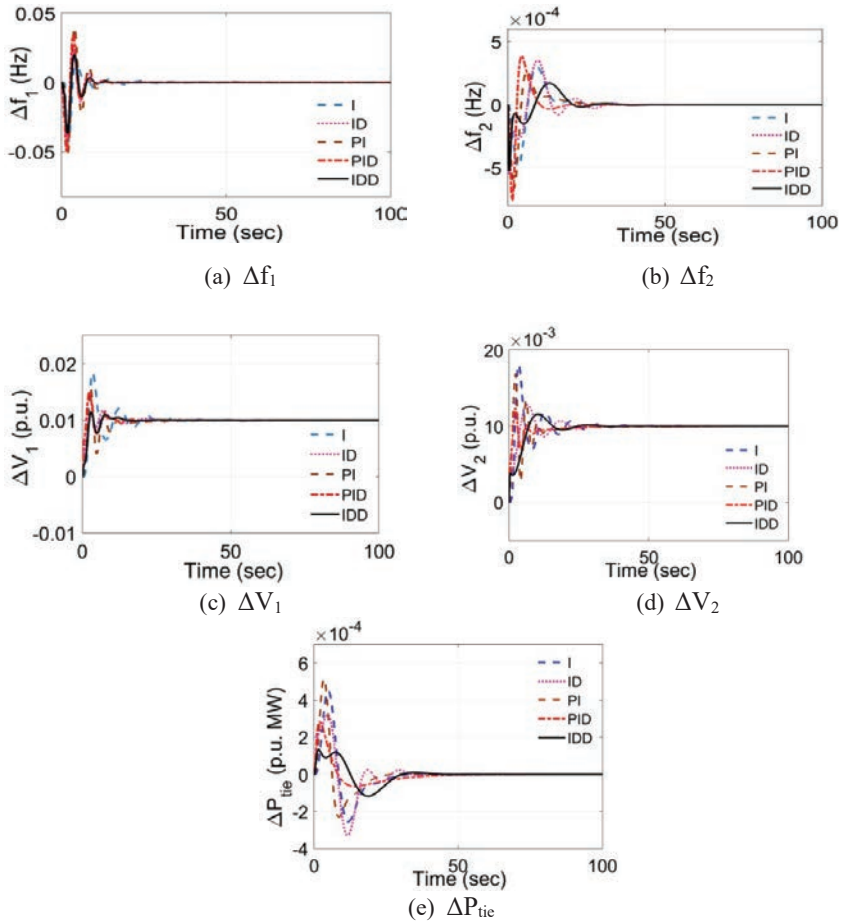

Figure 8 Dynamic responses comparison for MBO optimized controllers for I, ID, PI, PID and IDD controllers.

the convergence comparison of mentioned techniques in minimizing the designated objective-function represented by Equation (1). It is visibly clear that MBO possesses least values of ISE with respect to the other optimization techniques. This attains the objective 2 of Section 1.3.

The values of ISE (Equation (1)), are achieved for individual controllers and are depicted in Table 3. The comparison of obtained ISE values for each controller depicts that IDD exhibits least error with respect to the other controllers. This provides further attainment of objective 3 stated in Section 1.3.

Table 3 ISE of controllers used

Controller	ISE
I	0.0209
ID	0.0218
PI	0.0237
PID	0.0158
IDD	**0.0119**

Table 4 Characteristics evaluation of responses presented in Figure 8

Parameter	Controller	MO	MU	ToS	DI
Δf_1	I	0.04316	**−0.01735**	40	1600
	ID	0.04044	−0.02398	15	225
	PI	0.03944	−0.05088	15	225
	PID	0.03396	−0.05037	15	225
	IDD	**0.02042**	−0.03712	**14.08**	**198**
Δf_2	I	0.000301	**−0.00049**	34.99	1224
	ID	0.000354	−0.00056	43.2	1866
	PI	0.000382	−0.00067	37	1369
	PID	0.000536	−0.00056	35.64	1270
	IDD	**0.000172**	−0.00053	**30.87**	**953**
ΔV_1	I	0.01844	0	37.56	1411
	ID	0.01178	0	25.6	655
	PI	0.01574	0	29.77	886
	PID	0.01507	0	26.81	719
	IDD	**0.01141**	0	**15.94**	**254**
ΔV_2	I	0.01807	0	45.54	2074
	ID	0.01281	0	43.4	1884
	PI	0.01688	0	35.05	1229
	PID	0.01237	0	35.4	1253
	IDD	**0.01158**	0	**33.3**	**1109**
ΔP_{tie}	I	0.00045	−0.00026	32.09	1030
	ID	0.000322	−0.00033	36.83	1356
	PI	0.000513	−0.00023	34.2	1170
	PID	0.000283	**−0.00007**	42.36	1794
	IDD	**0.000134**	−0.00012	**30.74**	**945**

Table 4 displays the maximum values of overshoot (MO), undershoot (MU) and time to settle after disturbance from Figure 8 responses. Demerit Index (DI) is a metric for comparing the effectiveness of responses achieved with different controllers. Lesser the DI value, better will be the controller performance. DI value for a controller is considered by means of

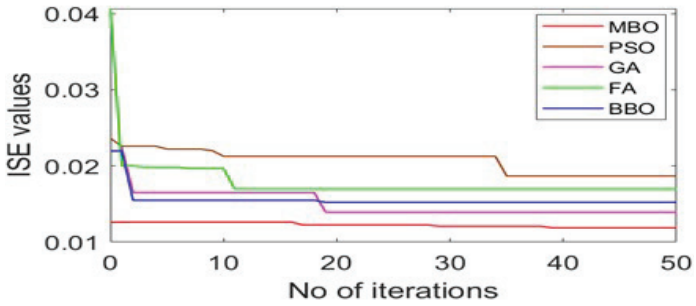

Figure 9 Convergence curves using different optimization techniques in present hybrid power system.

Equation (6). The DI value for each controller with respect to responses are presented in the last column of Table 4. Values given in Table 4 demonstrates the comparative enquiry of various controllers used in the present study. The predominance of IDD controller for the present power system with respect to MO, ToS and DI is evident from a close examination of these values. This study confirms and completes the attainment of objective 3 stated in Section 1.3.

$$DI = (MO)^2 + (MU)^2 + (ToS)^2 \tag{6}$$

3.2 EV's Role on System Dynamics (Objective 4 of Section 1.3)

To inspect the influence of EVs on system dynamics of developed system, EVs are detached from both areas. The dynamic responses when EVs are disconnected are achieved and paralleled with that achieved in absence of EVs (nominal system), presented in Figure 10. The critical analysis of Figure 10 reflects that the dynamic response deviations are suppressed more effectively in existence of EVs. This is due to the nature of high frequency components appearing in the power system are handled by EVs, resulting in a decline in regulatory procedures carried by generating components [15].

3.3 EV Power Management for System Regulation (Objective 5 of Section 1.3)

When the load in power system increases, frequency starts to decrease and vice-versa. The increase in load forces generating units to generate more power so as to attain the power balance. The analysis for EV power management is carried out based on the system dynamic responses demonstrated

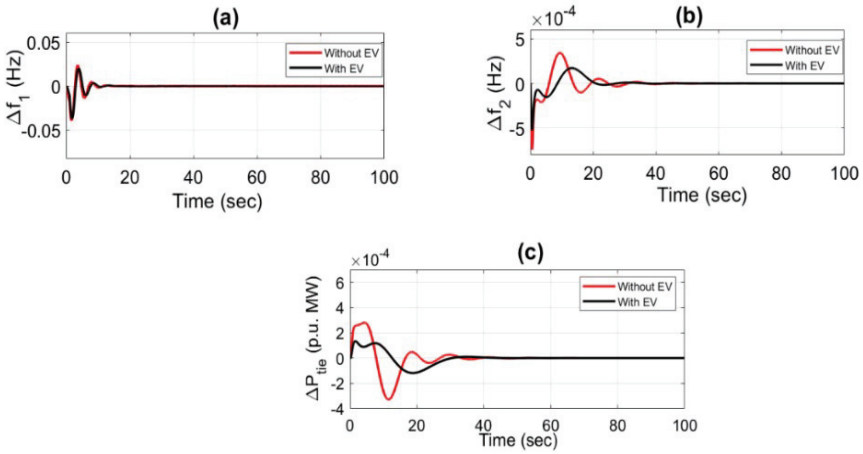

Figure 10 Response comparison for MBO optimized optimal controlled system in presence and absence of EVs (a) Δf_1 (b) Δf_2 (c) ΔP_{tie}.

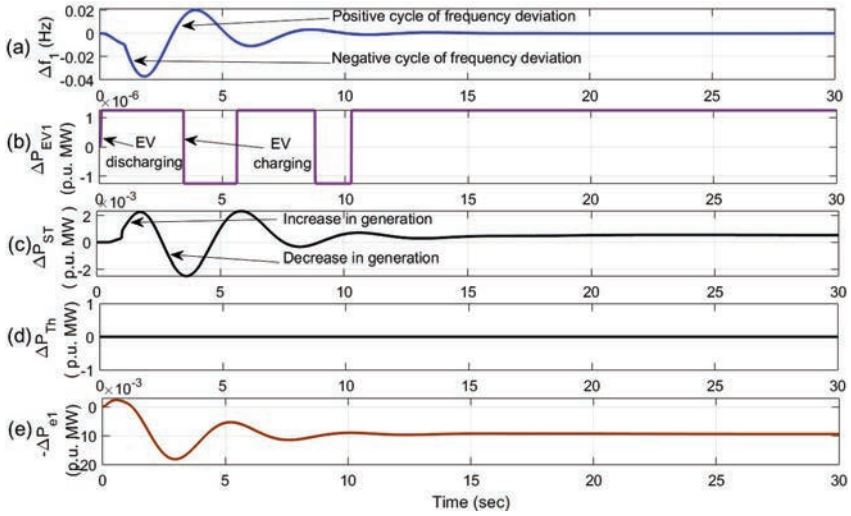

Figure 11 Response comparison for MBO optimized optimal controller in area-1 (a) Δf_1 (b) ΔP_{EV1} (c) ΔP_{ST} (d) ΔP_{Th} (e) ΔP_{e1}.

in Figure 8(a). The same is presented as Figure 11(a) showing the effect of load perturbation on the nominal system.

***Time 0–3 sec*:** This duration of Figure 11(a) depicts the negative cycle of frequency deviation, which implies increase in load demand of the system.

During this duration, as shown in Figure 11(b), EV increases the discharging power acting as a generating unit to raise the system frequency. As already reported in Section 2.1, the maximum and minimum power limit for EV is ± 5 kW. So, deviations in EV for area-1 are restricted to $\pm 1.25 \times 10^{-6}$ p.u. MW. Figures 11(c)–11(e) shows the power contribution of ST, CT and AVR in area-1. Due to slower dynamics, the conventional-thermal plant (Figure 11(d)) does not react to sudden change in load perturbation. On the other hand, the AVR loop being faster than LFC loop, responds quicker to the change in load perturbation. However, the contribution is very limited as shown in Figure 11(e) due to the fact that AVR loop is cross-coupled with LFC. Moreover, EV contributes power delivery upto its maximum limit. Thus, the additional generation for maintaining power balance is made available by solar-thermal plant as shown in Figure 11(c).

***Time 3–5 sec*:** This duration of Figure 11(a) depicts the positive cycle of frequency deviation, which implies surplus power generation in the system. During this, as shown in Figure 11(b), EV increases the charging power to reduce the system frequency and acts as an absorbing unit. The management of EV is thus carried on until the system frequency is brought to steady state.

3.4 Eigen Value Analysis (Objective 6 of Section 1.3)

Eigen value analysis gives the stability performance of a system. For a stable system, the Eigen values should lie on the left hand side (LHS) of imaginary axis. The transfer function models (Figures 2–3) are associated with 29 state variables. This analysis is performed with IDD as secondary controller in order to further validate the optimal operation of IDD controlled combined power system operation. Table 5 represents the state variables (29 numbers) with corresponding parameters. Table 6 shows the corresponding

Table 5 State variables and corresponding parameters of IDD controlled combined power system

$\boldsymbol{X}_1 = \Delta f_1$	$\boldsymbol{X}_2 = \Delta P_{DSTS1}$	$\boldsymbol{X}_3 = \Delta P_{R2}$	$\boldsymbol{X}_4 = \Delta P_{T1}$	$\boldsymbol{X}_5 = \Delta P_{G1}$	$\boldsymbol{X}_6 = \Delta P_{EV1}$	$\boldsymbol{X}_7 = \Delta P_{tie12}$
$\boldsymbol{X}_8 = \Delta P_{C1}$	$\boldsymbol{X}_9 = \Delta V_1$	$\boldsymbol{X}_{10} = \Delta \boldsymbol{X}_{e1}$	$\boldsymbol{X}_{11} = \Delta \boldsymbol{X}_{A1}$	$\boldsymbol{X}_{12} = \Delta \boldsymbol{X}_{S1}$	$\boldsymbol{X}_{13} = \Delta P_{C3}$	$\boldsymbol{X}_{14} = \Delta P_{e1}$
$\boldsymbol{X}_{15} = \Delta f_2$	$\boldsymbol{X}_{16} = \Delta P_{DSTS2}$	$\boldsymbol{X}_{17} = \Delta P_{R2}$	$\boldsymbol{X}_{18} = \Delta P_{T2}$	$\boldsymbol{X}_{19} = \Delta P_{G2}$	$\boldsymbol{X}_{20} = \Delta P_{EV2}$	$\boldsymbol{X}_{21} = \Delta P_{C2}$
$\boldsymbol{X}_{22} = \Delta V_2$	$\boldsymbol{X}_{23} = \Delta \boldsymbol{X}_{E2}$	$\boldsymbol{X}_{24} = \Delta \boldsymbol{X}_{A2}$	$\boldsymbol{X}_{25} = \Delta \boldsymbol{X}_{S2}$	$\boldsymbol{X}_{26} = \Delta P_{C4}$	$\boldsymbol{X}_{27} = \Delta \boldsymbol{X}_{AVR1}$	$\boldsymbol{X}_{28} = \Delta P_{e2}$
$\boldsymbol{X}_{29} = \Delta \boldsymbol{X}_{AVR2}$						

Table 6 Eigen values of IDD controlled system

$\boldsymbol{X}_1$	$-1.0000 + 0.0000$i	$\boldsymbol{X}_{15}$	$-5.2285 + 3.0422$i
$\boldsymbol{X}_2$	$-40.5749 + 0.0000$i	$\boldsymbol{X}_{16}$	$-5.2285 - 3.0422$i
$\boldsymbol{X}_3$	$-17.8634 + 2.2660$i	$\boldsymbol{X}_{17}$	$-4.5746 + 3.3908$i
$\boldsymbol{X}_4$	$-17.8634 - 2.2660$i	$\boldsymbol{X}_{18}$	$- 4.5746 - 3.3908$i
$\boldsymbol{X}_5$	$-14.1103 + 0.0000$i	$\boldsymbol{X}_{19}$	$-5.9803 + 0.0000$i
$\boldsymbol{X}_6$	$-12.5408 + 0.0000$i	$\boldsymbol{X}_{20}$	$-0.0596 + 2.8945$i
$\boldsymbol{X}_7$	$-1.5457 + 10.1397$i	$\boldsymbol{X}_{21}$	$-0.0596 - 2.8945$i
$\boldsymbol{X}_8$	$-1.5457 - 10.1397$i	$\boldsymbol{X}_{22}$	$-0.4992 + 0.0000$i
$\boldsymbol{X}_9$	$-1.6809 + 8.3787$i	$\boldsymbol{X}_{23}$	$-0.07607 + 0.0000$i
$\boldsymbol{X}_{10}$	$-1.6809 - 8.3787$i	$\boldsymbol{X}_{24}$	$-0.7132 + 0.0000$i
$\boldsymbol{X}_{11}$	$-1.6505 + 8.3450$i	$\boldsymbol{X}_{25}$	$-0.9989 + 0.0000$i
$\boldsymbol{X}_{12}$	$-1.6505 - 8.3450$i	$\boldsymbol{X}_{26}$	$-1.0000 + 0.0000$i
$\boldsymbol{X}_{13}$	$- 7.8140 + 1.1001$i	$\boldsymbol{X}_{27}$	$-20.0000 + 0.0000$i
$\boldsymbol{X}_{14}$	$-7.8140 - 1.1001$i	$\boldsymbol{X}_{28}$	$-17.2344 + 0.0000$i
$\boldsymbol{X}_{29}$	$-17.2344 - 0.0000$i		

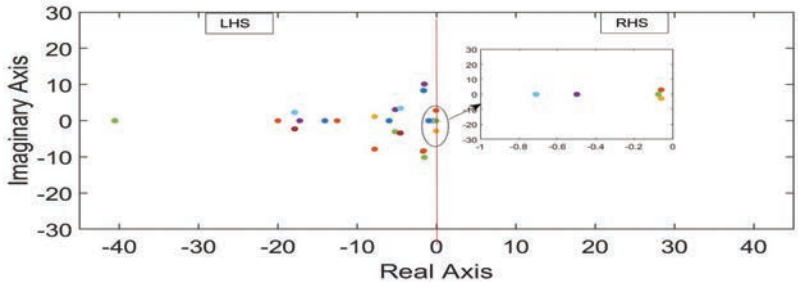

Figure 12 Plot of eigen values on imaginay axis.

Eigen values related to each system parameter. Table 6 clearly indicates that the Eigen values of IDD controlled combined power system have negative real parts, thereby authenticating stability of IDD controlled power system. This is depicted in Figure 12 where all the Eigen values lie on LHS of imaginary axis and no Eigen value lies on RHS of imaginary axis.

3.5 Sensitivity Analysis (SA) (Objective 7 of Section 1.3)

SA helps to inspect the strength of optimal controller gains for deviations in system parameters. The variations in system load and solar insolation are considered as the major parameters for the analysis.

SA is exhibited by exposing nominal system to deviations in load perturbations and solar irradiance. The responses pertaining to optimized gains

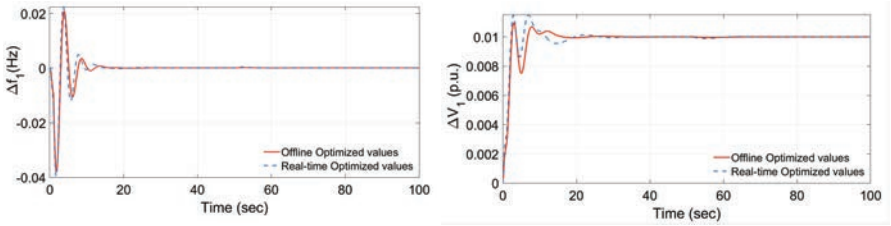

(a) Δf_1 (b) ΔV_1

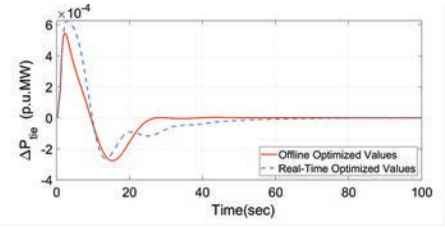

(c) ΔP_{tie}

Figure 13 Response comparison under 1% SLP in both areas.

of IDD-controller for varied values of nominal system labeled as *real-time optimized responses*. Moreover, previously obtained optimized responses the IDD controller for nominal system conditions, reported in Table 2, are labeled *offline optimized responses.*

3.5.1 Load-Perturbation of 1% in both areas

The developed system is supplied with 1% SLP in area-1 and area-2, as compared to 1% SLP (nominal condition) in area-1. The changed system is simulated and the dynamic responses are achieved and displayed in Figure 13. Table 7 reports the optimized gains of IDD controller in real-time. The observations from Figure 13 reflects that the offline and real-time optimized responses are merely same. Hence, it portrays the strength of optimized IDD controller gains.

3.5.2 Random-Load-Perturbation (RLP) in area-1

Area-1 of the present power system is altered with a more intricate load perturbation, which changes randomly as displayed in Figure 14(a). The goal is to analyze the strength of optimized IDD controller gains for intense load variations. As explained earlier, the real-time optimized values for IDD controller under the changed system conditions with respect to nominal

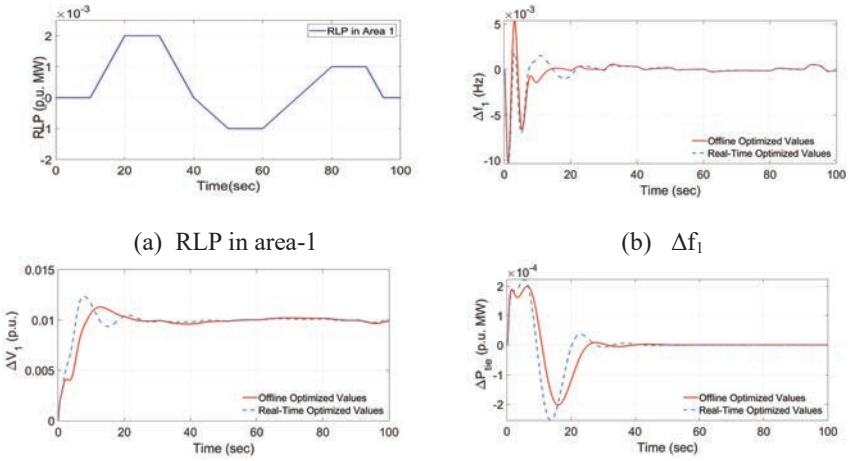

(a) RLP in area-1 (b) Δf_1

(b) ΔV_1 (c) ΔP_{tie}

Figure 14 Response comparison under Random load perturbation (RLP) in area-1.

Table 7 Optimized values under real-time for IDD controller for SLP of 1% in both area-1 and area-2

K_i	Value	K_d	Value	N	Value
K_{i1}	0.9216	K_{d11}	0.2151	N_{11}	30.3052
K_{i2}	0.2008	K_{d12}	0.4578	N_{12}	46.7483
K_{i3}	0.3035	K_{d21}	0.5170	N_{21}	84.3900
K_{i4}	0.6793	K_{d22}	0.4263	N_{22}	31.2881
		K_{d31}	0.4905	N_{31}	63.5388
		K_{d32}	0.1876	N_{32}	89.5250
		K_{d41}	0.1048	N_{41}	95.3827
		K_{d42}	0.9408	N_{42}	56.6585

system are obtained and reported in Table 9. The responses achieved for this case are presented in Figure 14. Table 8 shows the offline optimized values for IDD controller. From Figure 14, in the context of RLP variations, response evaluation yields a positive conclusion because both responses are almost identical. This indicates the effect of any random changes in load has very little effect on the reliability of the IDD-controlled power system.

3.5.3 Random variation in solar irradiance

Solar energy is easily available and is random in nature. To exhibit such practicality, this study incorporates a random discrepancy in solar irradiance

Table 8 Offline optimized values of IDD controller under nominal conditions

K_i	Value	K_d	Value	N	Value
K_{i1}	0.1908	K_{d11}	0.9881	N_{11}	89.8757
K_{i2}	0.4954	K_{d12}	0.3288	N_{12}	80.6318
K_{i3}	0.1698	K_{d21}	0.2846	N_{21}	54.9488
K_{i4}	0.399	K_{d22}	0.4514	N_{22}	68.4638
		K_{d31}	0.3254	N_{31}	52.5154
		K_{d32}	0.1805	N_{32}	57.8655
		K_{d41}	0.5074	N_{41}	59.6059
		K_{d42}	0.6672	N_{42}	39.7595

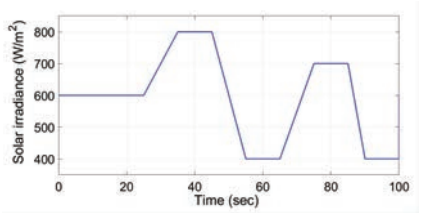

(a) Random solar irradiance

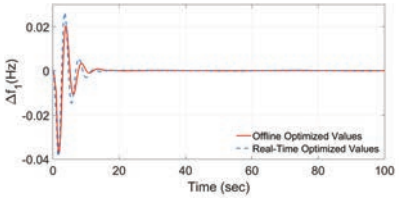

(b) Δf_1

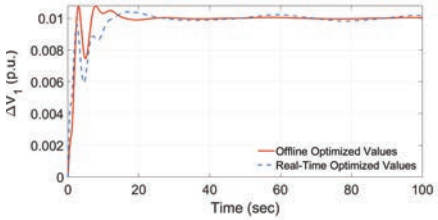

(b) ΔV_1

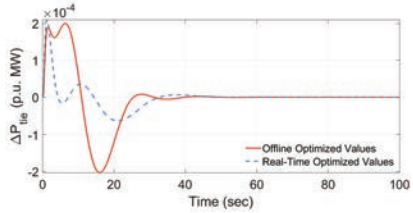

(c) ΔP_{tie}

Figure 15 Response comparison under random solar irradiance.

as presented in Figure 15(a). As explained earlier, the offline optimized values for IDD controller is as reported in Table 8. The real-time optimized values for IDD controller for this changed system conditions are obtained and represented in Table 10. The responses attained are displayed in Figure 15. The detailed inspection of Figure 15 infers the offline achieved responses are almost same as compared to the real-time optimized responses. Hence, the effect of change in solar irradiance has not led the power system in any type of instability. Thus, the studies in Section 3.5 completely confirm the attainment of objective 7 as stated in the Section 1.3.

Table 9 Optimized values under real-time for IDD controller for RLP in area-1

K_i	Value	K_d	Value	N	Value
K_{i1}	0.3425	K_{d11}	0.2719	N_{11}	33.5725
K_{i2}	0.7274	K_{d12}	0.5125	N_{12}	22.1575
K_{i3}	0.3120	K_{d21}	0.9715	N_{21}	16.6120
K_{i4}	0.5317	K_{d22}	0.0609	N_{22}	31.1702
		K_{d31}	0.2499	N_{31}	35.6891
		K_{d32}	0.2167	N_{32}	32.3934
		K_{d41}	0.2792	N_{41}	27.8019
		K_{d42}	0.8260	N_{42}	29.5555

Table 10 Optimized values under real-time for IDD controller for random solar irradiance

K_i	Value	K_d	Value	N	Value
K_{i1}	0.6763	K_{d11}	0.3646	N_{11}	11.0809
K_{i2}	0.9497	K_{d12}	0.9931	N_{12}	85.1211
K_{i3}	0.1322	K_{d21}	0.1922	N_{21}	3.6262
K_{i4}	0.1594	K_{d22}	0.4200	N_{22}	33.3548
		K_{d31}	0.7745	N_{31}	69.2600
		K_{d32}	0.4276	N_{32}	9.3941
		K_{d41}	0.6710	N_{41}	88.2859
		K_{d42}	0.9789	N_{42}	47.0951

4 Conclusion

Implementation & effective operation of electric vehicles in improving the system dynamics of a hybrid power system using an optimal IDD control. The secondary controllers are effectively optimized utilizing an efficient MBO technique. The performance of optimally controlled system in terms of maximum values of overshoot, undershoot, time to settle after disturbance (ToS) and demerit index (DI) confirms the dominance of optimal IDD-controller in contrast to other conventional controllers. Results show a reduction of 25% in steady state errors and a mean of 32% reduction in DI. The stability of the optimal IDD controlled system is further verified by Eigen-value analysis. The role of EV in supplying electrical energy as well as acting as energy storage has been successfully demonstrated. A more complex work can be carried out by implementing more practical scenarios for case studies related to present work. This work can lead the researchers to explore further possible optimal options in collective LFC-AVR power system operation incorporating EV and renewables.

Appendix: Nominal Parameters of System:

LFC system							
Frequency (f): 60 Hz	H_i: 5s	D_i: 8.33 $\times$ 10^{-3} p.u. MW/Hz	R_i: 2.4 Hz/p.u. MW				
a_{12}: $-2/3$	loading: 50%	T_{pi}: 20s	K_{DSTS}: 1			T_{DSTS}: 1;	
N_{EVi}: 1	K_{EVi}: 1	T_{EVi}: 1 s	$Bias_i = \beta_i$: 0.425 p.u. MW/Hz				
T_{gi}: 0.08 s	T_{ti}: 0.3 s	T_{ri}: 10 s	K_{ri}: 0.5			K_{pi}: 120 Hz/(p.u. MW)	
$apf_{11} = 0.3$	$apf_{12} = 0.6$	$apf_{13} = 0.1$	$apf_{21} = 0.1$			$apf_{22} = 0.8$	$apf_{23} = 0.1$
AVR System							
K_{A1}: 10	T_{A1}: 0.1 s	K_{E1}:1	K_{S1}:1	T_{E1}:0.4 s	T_{S1}:0.05 s	K_{F1}:0.8	T_{F1}:1.4 s

Acknowledgement

The authors are thankful to NIT Srinagar for providing the scholarship and lab facilities for carrying out this work.

References

[1] T. Wu, S. Bu , X. Wei , G. Wang , B. Zhou, "Multitasking multi-objective operation optimization of integrated energy system considering biogas-solar-wind renewables," Energy Conversion and Management , 229, 2021, doi.org/10.1016/j.enconman.2020.113736.

[2] F. Ren, J. Wang, S. Zhu, Y. Chen, "Multi-objective optimization of combined cooling, heating and power system integrated with solar and geothermal energies," Energy Conversion and Management, Volume 197, 2019, 111866, ISSN 0196-8904, https://doi.org/10.1016/j.enconman.2019.111866.

[3] C.E. Fosha, O.I. Elgerd, "The Megawatt-Frequency Control Problem: A New Approach Via Optimal Control Theory," IEEE Transactions on Power Apparatus and Systems, vol. 89(4), pp. 563–577, 1970. doi: 10.1109/TPAS.1970.292603.

[4] Farooq Z, Rahman A, Lone SA. Load frequency control of multi-source electrical power system integrated with solar-thermal and electric vehicle. International Transactions on Electrical Energy Systems. 2021 May 6:e12918.

[5] Farooq Z, Rahman A, Lone SA. System dynamics and control of EV incorporated deregulated power system using MBO-optimized cascaded ID-PD controller. International Transactions on Electrical Energy Systems. 2021 Nov;31(11):e13100.

[6] Farooq Z, Rahman A, Hussain SM, Ustun TS. Power Generation Control of Renewable Energy Based Hybrid Deregulated Power System. Energies. 2022 Jan;15(2):517.

[7] Farooq, Z, Rahman, A, Lone, SA. Power generation control of restructured hybrid power system with FACTS and energy storage devices using optimal cascaded fractional-order controller. Optim Control Appl Meth. 2022; 1–30. doi: 10.1002/oca.2850.

[8] A. Rahman, L.C. Saikia, N. Sinha, "Automatic generation control of an interconnected two-area hybrid thermal system considering dish-stirling solar thermal and wind turbine system," Renewable Energy, Volume 105, Pages 41–54, 2017. ISSN 0960-1481.

[9] A. Rahman, S.K. Sahu, L.C. Saikia, P. Dash, "AGC of a multi-area thermal-CCGT system using Cuckoo Search optimized classical controllers," International Conference on Energy, Power and Environment: Towards Sustainable Growth (ICEPE), Shillong, pp. 1–6, 2015. doi: 10.1109/EPETSG.2015.7510099.

[10] Y. Wei, I. Jayawardene, G. K. Venayagamoorthy, "Optimal automatic generation controllers in a multi-area interconnected power system with utility-scale PV plants," IET Smart Grid, vol. 2(4), pp. 581–593, 2019. doi: 10.1049/iet-stg.2018.0238.

[11] A. Rahman, L.C. Saikia, N. Sinha, "Load frequency control of a hydro-thermal system under deregulated environment using biogeography-based optimised three-degree-of-freedom integral-derivative controller," IET Generation, Transmission & Distribution, vol. 9(15), pp. 2284–2293, 2015. doi: 10.1049/iet-gtd.2015.0317.

[12] S. Sondhi, Y. V. Hote, "Fractional order PID controller for load frequency control," Energy Conversion and Management, Volume 85, 2014, Pages 343–353, ISSN 0196-8904, doi.org/10.1016/j.enconman.2014.05.091.

[13] W. Tan, "Decentralized load frequency controller analysis and tuning for multi-area power systems," Energy Conversion and Management, Volume 52, Issue 5, 2011, Pages 2015–2023, ISSN 0196-8904, https://doi.org/10.1016/j.enconman.2010.12.011.

[14] R. Rajbongshi, L.C. Saikia, "Combined voltage and frequency control of a multi-area multisource system incorporating dish-Stirling solar

thermal and HVDC link," IET Renewable Power Generation, vol. 12(3), pp. 323–334, 2018. doi: 10.1049/iet-rpg.2017.0121.

[15] Safiullah S, Rahman A, Lone SA. State-observer based IDD controller for concurrent frequency-voltage control of a hybrid power system with electric vehicle uncertainties. International Transactions on Electrical Energy Systems. 2021 Nov;31(11):e13083.

[16] Safiullah S, Rahman A, Ahmad Lone S. Optimal control of electrical vehicle incorporated hybrid power system with second order fractional-active disturbance rejection controller. Optimal Control Applications and Methods. 2021 Nov 25.

[17] H.N. de Melo, J.P.F. Trovão, P.G. Pereirinha, H.M. Jorge, C.H. Antunes, "A Controllable Bidirectional Battery Charger for Electric Vehicles with Vehicle-to-Grid Capability," IEEE Transactions on Vehicular Technology, vol. 67(1), pp. 114–123, 2018. doi: 10.1109/TVT.2017.2774189.

[18] W. Lee, L. Xiang, R. Schober, V.W.S. Wong, "Electric vehicle charging stations with renewable power generators: A game theoretical analysis," IEEE Power & Energy Society General Meeting, Denver, CO, pp. 1–1, 2015. doi: 10.1109/PESGM.2015.7286014.

[19] R. Abousleiman, R. Scholer, "Smart Charging: System Design and Implementation for Interaction between Plug-in Electric Vehicles and the Power Grid," IEEE Transactions on Transportation Electrification, vol. 1(1), pp. 18–25, 2015. doi: 10.1109/TTE.2015.2426571.

[20] A. Saha, L.C. Saikia, Lalit, "Renewable energy source-based multiarea AGC system with integration of EV utilizing cascade controller considering time delay," International Transactions on Electrical Energy Systems, vol. 29, 2018. doi: 10.1002/etep.2646.

[21] H. Liu, K. Huang, Y. Yang, H. Wei, S. Ma, "Real-time vehicle-to-grid control for frequency regulation with high frequency regulating signal," Protection and Control of Modern Power Systems 3, pp. 1–8, 2018.

[22] F. Kennel, D. Görges, S. Liu, "Energy Management for Smart Grids With Electric Vehicles Based on Hierarchical MPC," IEEE Transactions on Industrial Informatics, vol. 9, no. 3, pp. 1528–1537, Aug. 2013, doi: 10.1109/TII.2012.2228876.

[23] M.A. Hannan, F.A. Azidin, A. Mohamed, "Multi-sources model and control algorithm of an energy management system for light electric vehicles," Energy Conversion and Management, Volume 62, 2012, Pages 123–130, ISSN 0196-8904, doi.org/10.1016/j.enconman.2012.04.001.

[24] A. Rahman, L.C. Saikia, N. Sinha, "Maiden application of hybrid pattern search-biogeography based optimisation technique in automatic generation control of a multi-area system incorporating interline power flow controller," IET Generation, Transmission & Distribution, vol. 10(7), pp. 1654–1662, 2016. doi: 10.1049/iet-gtd.2015.0945.

[25] R. K. Sahu, S. Panda, and S. Padhan, "Optimal gravitational search algorithm for automatic generation control of interconnected power systems," Ain Shams Eng. J., vol. 5, pp. 721–733, 2014.

[26] J. Morsali, K. Zare, and M. T. Hagh, "Applying fractional order PID to design TCSC-based damping controller in coordination with automatic generation control of interconnected multi-source power system," Eng. Sci. Technol. Int. J., vol. 20, pp. 1–17, 2017.

[27] D. Kler, V. Kumar and K.P.S. Rana, "Optimal integral minus proportional derivative controller design by evolutionary algorithm for thermal-renewable energy-hybrid power systems," IET Renewable Power Generation, vol. 13 (11), pp. 2000–2012, 2019. doi: 10.1049/iet-rpg.2018.5745.

[28] S. Debbarma, L.C. Saikia, and N. Sinha, "Solution to automatic generation control problem using firefly algorithm optimized Iλ Dμ controller," ISA Trans., vol. 53, pp. 358–366, 2014.

[29] A. Behera, T.K. Panigrahi, P.K. Ray, A.K. Sahoo, "A novel cascaded PID controller for automatic generation control analysis with renewable sources," IEEE/CAA Journal of Automatica Sinica, vol. 6(6), pp. 1438–1451, 2019. doi: 10.1109/JAS.2019.1911666.

[30] N. Veerasamy,N. Wahab, R. Ramachandran, M. Othman, H. Hizman, A. Irudayaraj, M. Guerrero,J. Kumar. A Hankel. "Matrix based reduced order model for stability analysis of hybrid power system using PSO-GSA optimized cascade PI-PD controller for automatic load frequency control," IEEE Access, vol. 8, pp. 71422–71446, 2020.

[31] P. Dash, L. C. Saikia, N. Sinha, "Automatic generation control of multi area thermal system using Bat algorithm optimized PD–PID cascade controller, "International Journal of Electrical Power & Energy Systems, vol. 68, pp. 364–372, 2015. ISSN 0142-0615. https://doi.org/10.1016/j.ijepes.2014.12.063.

[32] A. Rahman, L.C. Saikia, N. Sinha, "Load frequency control of a hydro-thermal system under deregulated environment using biogeography-based optimised three-degree-of-freedom integral-derivative controller," IET Generation, Transmission & Distribution, vol. 9(15), pp. 2284–2293, 2015. doi: 10.1049/iet-gtd.2015.0317.

[33] J.R. Nayak, B. Shaw, B.K. Sahu, "Implementation of hybrid SSA–SA based three-degree-of-freedom fractional-order PID controller for AGC of a two-area power system integrated with small hydro plants," IET Generation, Transmission & Distribution, vol. 14 (13), pp. 2430–2440, 2020. doi: 10.1049/iet-gtd.2019.0113.

[34] H. Mo and L. Xu, "Magnetotactic bacteria optimization algorithm for multimodal optimization," IEEE Symposium on Swarm Intelligence (SIS), Singapore, pp. 240–247, 2013. doi: 10.1109/SIS.2013.6615185.

[35] L. C. Saikia, J. Nanda, S. Mishra, "Performance comparison of several classical controllers in AGC for multi-area interconnected thermal system," International Journal of Electrical Power & Energy Systems, vol. 33(3), pp. 394–401, ISSN 0142-0615, 2011. https://doi.org/10.1016/j.ijepes.2010.08.03.

Biographies

Sheikh Safiullah was born in Pulwama, Jammu and Kashmir on April 5, 1992. He graduated from Baba Ghulam Shah Badshah University Rajouri, J & K, India in 2015. His has a teaching at National Institute of Technology, Srinagar, India. Safiullah received MTech from Sharda University Greater Noida, Uttar Pradesh, India in 2017. He is presently pursuing doctorate in Electrical engineering at National Institute of Technology, Srinagar, India. His special fields of interest include load frequency control, Power system Control (AGC & AVR) applications, Grid, Renewable, Soft computing Techniques.

Asadur Rahman did his Ph. D from NIT Silchar, India in Power & Energy systems specialization. He was the Batch Topper of M. Tech EE (Power & Energy Systems) at NIT Silchar. He is presently serving as an Assistant Professor at NIT Srinagar and was previously associated with NIT Nagaland, NIT Mizoram and GIMT Guwahati. He is an active member of many professional bodies viz. IEEE, ISTE, I.E (I), SESI, and SCRS. His research interests include Electrical Power System Control, Power System Optimization, Smart-Grid, Micro-Grid, Integration of EVs, Renewable Energy Systems, and Soft Computing Techniques. He is reviewer to many reputed journals and his research articles are published in international journals of repute like IET-GTD, IET-RPG and Elsevier-RENE.